*Journal of Applied Electrochemistry* **34**: 305–314, 2004.



# Study of anodic layers and their effects on electropolishing of bulk and electroplated films of copper

J. HUO[1,*], R. SOLANKI[1] and J. McANDREW[2]
[1]*Department of Electrical and Computer Engineering, OGI School of Science and Engineering at OHSU, Beaverton, OR 97006, USA*
[2]*Electronics R&D Group, Air Liquide, Countryside, IL 60525, USA*
*(*author for correspondence, e-mail: jinshan_huo@yahoo.com)*

Received 9 May 2003; accepted in revised form 11 October 2003

*Key words:* copper electropolishing, electrochemical impedance spectroscopy, mass transport, migration smoothing, ohmic levelling.

**Abstract**

Copper anodic layers in solutions of hydroxyethylidenediphosphonic acid (HEDP), phosphoric acid, and phosphoric acid with organic and inorganic additives were analysed *in situ* using electrochemical impedance spectroscopy (EIS). Salt films formed in HEDP solutions were detected. No salt film was found in solutions of phosphoric acid or phosphoric acid with copper oxide, ethylene glycol and sodium tripolyphosphate as additives. Analysis of EIS data suggests that $H_2O$ molecules are the mass transport controlling species in solutions of phosphoric acid and of phosphoric acid with copper oxide, whereas $Cu^{2+}$ ions are the mass transport controlling species in solutions of HEDP and of phosphoric acid with additives ethylene glycol and sodium tripolyphosphate. Very good results for electropolishing of bulk copper discs were obtained in all the above solutions, but the electropolishing of electroplated copper films on patterned silicon wafers is more challenging. In this case, good planarization was obtained only from HEDP solutions. Experimental results and theoretical analysis indicate that surface profile of anodic layers is an important factor influencing planarization of electroplated copper films on patterned silicon wafers. An electrically resistive anode film with macro surface profile can lead to planarization of the gentle surface undulations of electroplated copper films on trenched silicon wafers due to migration smoothing, diffusion smoothing, and ohmic levelling effects.

## 1. Introduction

Damascene is the most common technique used for fabricating copper interconnects in microelectronic devices. In this method, a thick Cu film is deposited, generally employing electroplating to fill barrier layer coated vias and trenches in an interlayer dielectric (ILD). The excess Cu is removed using chemical mechanical polishing (CMP), leaving the recessed structures filled with Cu. To reduce the capacitance between interconnects, a lower dielectric constant ILD is required. At present, carbon-doped silica (SiOC) films formed by CVD are competing with polymeric spin-on dielectric (SOD) films to replace the current standard fluorosilicate glass (FSG) films. Both of the new types of materials are softer than FSG. Future device generations will require yet lower dielectric constant ILDs, which can be achieved by introducing porosity into the films. Unfortunately, this makes the ILD even softer. Both SiOC and polymeric SOD films are too soft to be easily integrated with CMP, and future porous materials will be even more difficult. Hence, alternate polishing techniques are urgently needed. One possible solution is electrochemical polishing (ECP).

It is known that ECP effect can be produced through brightening (or microsmoothing) and levelling (or macrosmoothing). Levelling results from the fact that protruding parts of a rough surface dissolve faster than recessed parts [1, 2]. This can be achieved under ohmic or mass transport control [3]. Brightening can be achieved only under mass transport control, which suppresses crystallographic etching [1, 3–5].

There are three types of mass transport limiting species: the cation of dissolving metal ($M^{n+}$) in the anodic salt film, the electrolyte anion ($A^{m-}$), and water molecules in the diffusion layer between anode and bulk solution [3]. However, details of the ECP mechanisms are unknown. Additionally, more challenges arise when the ECP technique is applied to copper films plated on patterned silicon wafers [6–8]. The patterned features of electroplated copper films are difficult to remove and may lead to nonuniform polishing. It was also found that ECP efficiency was influenced by the patterned features on the substrate surface [9].

Anode surface layers play a critical role in mass transport in an ECP process. Chang et al. [10] argued that a porous anodic layer was present on the copper surface in their study of ECP of patterned wafers in phosphoric acid. However, in a previous study using the same electrolyte, Vidal and West [11] concluded that mass transport was limited by an acceptor mechanism (with water as the most likely acceptor molecule) rather than by a physical layer. Probing of the anode layer is very challenging since it may break down when the potential is switched off and the anode is taken out of the electrolyte. Electrochemical impedance spectroscopy (EIS) has been used to study iron alloys and copper anode layers in $H_3PO_4$–$H_2SO_4$, $FeCl_2$, and $H_3PO_4$ electrolytes [5, 11–13].

Our objective was to investigate copper anodic layers in various solutions that may be used for electropolishing Cu for microelectronic applications. Hence, copper anodic layers formed in various solutions were detected using *in situ* EIS. The effects of anodic layers on mass transport and ECP have been studied, as well as the influence of surface profiles on polishing efficiency.

## 2. Experimental details

### 2.1. *Analysis of copper anodic layer with electrochemical impedance spectroscopy*

AC impedance analysis of copper anodic layer was carried out in aqueous solutions of hydroxyethylidenediphosphonic acid (HEDP), phosphoric acid, and phosphoric acid with copper oxide, ethylene glycol and sodium tripolyphosphate, listed in Table 1. The analysis system consisted of Princeton Applied Research 273A potentiostat/galvanostat and Solartron SI 1260 impedance/gain-phase analyser. The details of the set-up are shown in Figure 1(a). The samples used were copper (99.99% Cu) discs of surface area 1 $cm^2$ and thickness 1.5 mm. A 12 mm thick and 43 mm diameter copper plate served as a cathode. The measurements were performed with 'controlled E sweep frequency' under the following conditions: controlled d.c. voltage, a.c. signal of 10 mV and frequency range of 100 kHz to 0.1 Hz; 100 mL solution in a 200 mL glass container; 100 rpm anode rotating speed; and room temperature. Before each measurement, a 50 s pretreatment (i.e., applied the d.c. voltage to the anode while a.c. voltage is zero) was performed.

### 2.2. *Electrochemical polishing of copper discs and EP copper films on silicon wafers*

ECP of copper discs and copper films on deep trench wafer coupons was performed with computer-controlled chronoamperometry. The controlled potentials were the middle points of the limiting current plateau ($E_L$) on the polarization curves, which were measured beforehand [14]. For this study, copper films were produced by electroplating 200 mm diameter deep trench wafers. The system used for ECP of copper discs was same as the one for impedance measurements, except that the impedance/gain-phase analyser was not connected. A customized sample holder was fabricated to hold 5 cm × 5 cm wafer coupons for ECP. A larger cylindrical container (~3 L), that included a cathode and a conical filter were also used (Figure 1(b)). 1300 mL solution was used for ECP of each wafer coupon. The reason for using the conical filter was to block hydrogen bubbles from reaching the anode surface. Surface

*Table 1.* Summary of measured impedance data

| Solution | Potential /V | $R_1$ /Ω $cm^2$ | $R_2$ /Ω $cm^2$ | $C_d$ /μF $cm^{-2}$ |
|---|---|---|---|---|
| 1. 100% phosphoric acid | 0.25 | 7.5 | 0.5 | 906 |
| | 1.25 | 7.5 | 9.0 | 11 |
| | 1.5 | 7.5 | 9.0 | 14 |
| | 1.6 | 7.5 | 9.0 | 18 |
| 2. 70% phosphoric acid | 0.25 | 7.6 | 0.4 | 199 |
| + 1.2 M CuO | 1.0 | 7.6 | 3.4 | 12 |
| | 1.5 | 7.6 | 3.4 | 74 |
| 3. 50% phosphoric acid | 0.25 | 29.0 | – | – |
| + 50% ethylene glycol | 1.5 | 29.0 | 13.0 | 12 |
| | 1.8 | 29.0 | 15.0 | 11 |
| | 2.0 | 29.0 | 20.0 | 80 |
| 4. 70% HEDP | 0.25 | 6.0 | 14.0 | 180 |
| | 1.3 | 7.0 | 4.0 | 20 |
| | 1.6 | 8.0 | 4.5 | 11 |
| 5. 70% phosphoric acid +0.5 | 0.25 | 8.0 | 9.0 | 88 |
| M sodium tripolyphosphate | 1.5 | 8.0 | 5.0 | 13 |
| | 2.0 | 8.0 | 7.0 | 29 |

Note: phosphoric acid = 85% $H_3PO_4$.

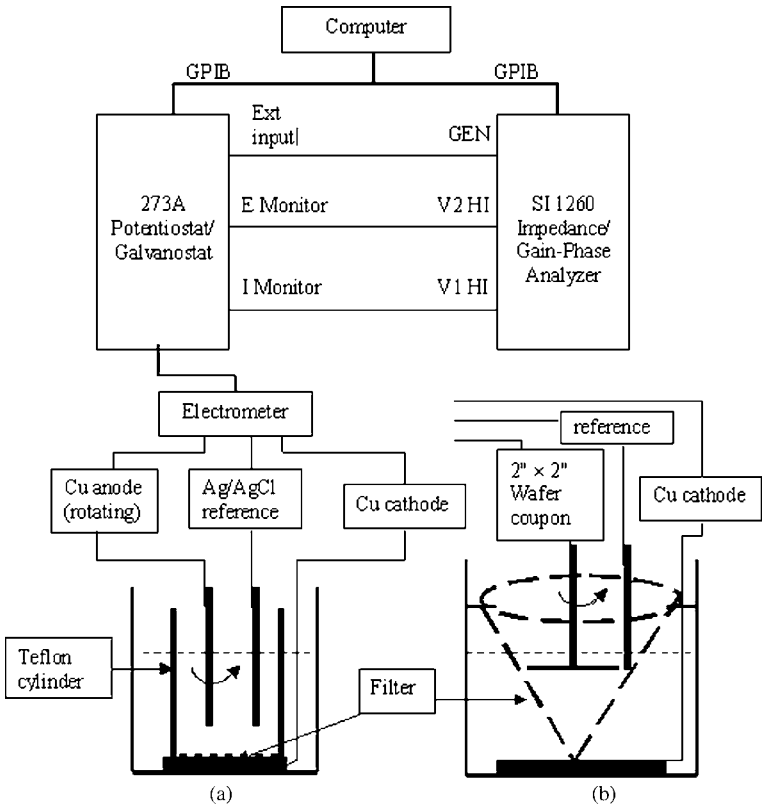


*Fig. 1.* (a) Configuration of electrochemical impedance spectroscopy (EIS) system and (b) silicon wafer holder.

profiles of the samples before and after ECP were examined with an atomic force microscope (AFM), optical and electron microscopes, as well as a surface profilometer.

## 3. Results and discussion

### 3.1. *Electrochemical impedance spectra*

To understand an electrochemical impedance spectrum, mass transport processes in the electrolyte and the possible structures of the anode–electrolyte interface must be understood. In an electrochemical cell with a rotating disc electrode (RDE) and/or circulated aqueous solution, the primary mechanisms for mass transport of ions between anode and cathode are ion migration, convection and diffusion processes driven by an electrical field, pressure, and concentration gradient, respectively [15].

The thickness of the hydrodynamic boundary layer can be determined from [16]

$$\delta = \frac{5x}{\sqrt{Re_x}} \tag{1}$$

where $Re_x \equiv \rho u_\infty x/\mu$ is the Reynolds number (in range $1 \times 10^5 \sim 3 \times 10^6$ for flow over flat plate), $\rho$ is the density (kg m$^{-3}$) of the solution, $u_\infty$ is the fluid velocity (m s$^{-1}$) in bulk solution outside the boundary layer, $x$ is the characteristic length in the flow direction, and $\mu$ is the viscosity (kg s$^{-1}$ m$^{-1}$). For our experimental conditions, $\delta$ was estimated to be between 30$\sim$ 160 $\mu$m. Outside the boundary layer, mass transport is dominated by convection. Inside the boundary layer, convection is weak and mass transport is dominated by diffusion and migration (if a potential difference exists). The ratio of migration to diffusion depends on electrochemical reaction and the conductance of ions in the solution [17].

In an electrochemical system, if charge transfer and chemical reaction processes are slower than diffusion and migration, there will be zero concentration gradient in the boundary layer. However, if a potential applied to the anode is within the range of the limiting current plateau, then mass transport may become the controlling process and a concentration gradient can develop (Figure 2(a)). The thickness of the diffusion/migration layer, for a RDE and considering only diffusion, is [18]

$$\delta_c = 1.61\, D^{1/3} v^{1/6} \omega^{-1/2} \tag{2}$$

where $D$ is the diffusion coefficient (cm$^2$ s$^{-1}$), $v = \mu/\rho$ is kinematic viscosity (cm$^2$ s$^{-1}$), and $\omega$ is angular frequency of rotation (s$^{-1}$).

Further, if a salt film is formed on the anode surface, the adjacent film and a diffusion layer may work together as a diffusion/migration barrier, which limits the diffusion/migration of the dissolved metal cations ($M^{n+}$) from anode to bulk solution. As a result, more complicated concentration gradient profiles may develop, as shown in Figure 2(b). The concentration gradient profiles depend on ion migration and diffusion resistances.

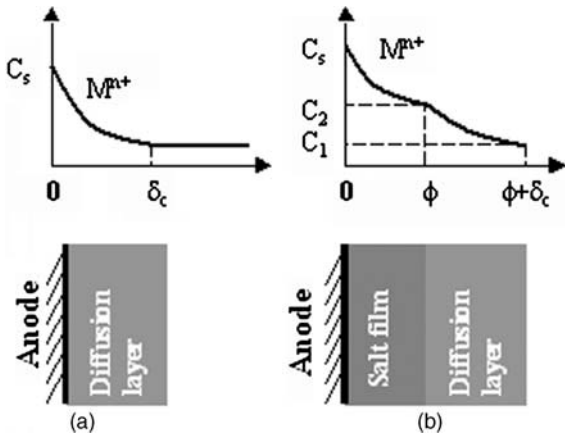


*Fig. 2.* Concentration gradient profile in (a) boundary layer and (b) in salt a film and boundary layer.

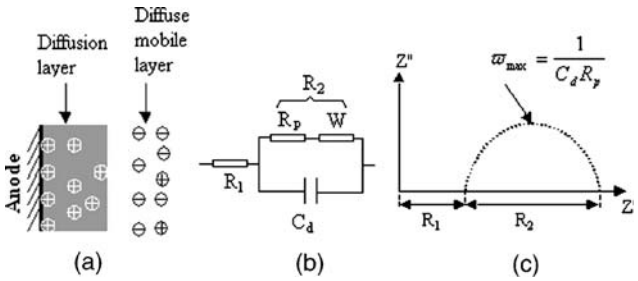


*Fig. 3.* (a) Diffused mobile layer, (b) equivalent circuit of an electrode with diffusion layer (b) and (c) the impedance plot.

The $M^{n+}$ cations in the salt film/diffusion layer attract nearby anions ($A^{m-}$) in the solution. The negative ions form a diffused mobile layer (Figure 3(a)), which is balanced by the attraction from $M^{n+}$ ions in the salt film/diffusion layer and the repulsion from electrons in the anode. This structure is similar to the 'double layer' and it behaves like a capacitor ($C_d$) under a.c. signal. Thus the equivalent circuit of the electrochemical cell may be represented as in Figure 3(b), for which

$$R_1 = R_m + R_e + R_f \tag{3}$$

$$R_2 = R_p + W \tag{4}$$

Here, $R_m$ is the resistance of the connections between electrodes and power/control units, $R_e$ and $R_f$ are the ohmic resistance of the electrolyte and the salt film, respectively; $R_p$ is polarization resistance, and $W$ is Warburg impedance corresponding to the diffusion process. Then, the total a.c. impedance is [19] given by

$$Z = R_1 + \frac{R_2}{1 + (\bar{\omega} C_d R_2)^2} - j\frac{\bar{\omega} C_d R_2^2}{1 + (\bar{\omega} C_d R_2)^2} = Z' + jZ'' \tag{5}$$

where $\bar{\omega}$ is the angular frequency of the a.c. signal. A Nyquist plot ($Z' \sim Z''$) corresponding to Equation 5 is shown in Figure 3(c).

Some of the measured impedance spectra of a copper anode in HEDP solution and phosphoric acid solutions with and without additives are shown in Figure 4. At high frequency, a semicircle was obtained at all the d.c. potentials for all the solutions. At low frequency range, the EIS line shifts left with increase in applied d.c. potential for solutions 2, 3 and 5. Similar behavior was reported by Vidal and West in [11]. This phenomenon is not prominent for solution 1. For solution 4 (HEDP), a reverse trend was observed over the range of limiting current plateau.

$R_1$, $R_2$ and $C_d$ data were extracted from the spectra according to their definitions illustrated in Figure 3(c). These values are listed in Table 1. All the potentials in Table 1, except 0.25 V, are in the range of the limiting current plateau. Since 0.25 V is far below the potential range of the limiting current plateau, no anodic film can be formed. Thus, according to the above discussion, $R_1$ obtained at 0.25 V is

$$R_1(0.25\,\mathrm{V}) = R_m + R_e \tag{6}$$

where $R_m$ is a constant, and $R_e$ is a constant for a given solution. Table 1 shows that concentrated phosphoric acid and its solutions with additives copper oxide, ethylene glycol, and sodium tripolyphosphate, all have a constant value of $R_1$ at all the tested potentials.

In contrast, the copper–HEDP system has different values of $R_1$ at all three applied potentials (Figure 4(b)): $R_1(0.25\ \mathrm{V}) = R_m + R_e = 6\ \Omega$, $R_1(1.3\ \mathrm{V}) = 7\ \Omega$, $R_1$ $(1.6\ \mathrm{V}) = 8\ \Omega$. Substituting these values into Equation 3, gives the resistance of the anodic layer in the Cu–HEDP system:

$$R_f(1.3\,\mathrm{V}) = 1\,\Omega$$

$$R_f(1.6\,\mathrm{V}) = 2\,\Omega.$$

This suggests the existence of a salt film in Cu–HEDP system; its thickness increases with increasing potential. In the case of phosphoric acid solutions studied in this investigation, the $R_1$ values indicate that no salt film was formed on the copper anode surface. The results for HEDP solution and concentrated phosphoric acid agree with previous studies [20–22]. XPS [21] indicated that the composition of the salt film is close to $[Cu_4(PO_4)$-HEDP$]_n$.

On the one hand, at a potential lower than the limiting current plateau, the process is mainly charge transfer and/or chemical reaction controlled. So $R_2$ (0.25 V) is mainly polarization resistance $R_p$. On the other hand, over the range of the limiting current plateau, Warburg impedance ($W$) may play a much more important role. The values of $R_2$ in Table 1 indicate that in solutions 3, 4 and 5 it increased with an increase of potential within the range of the limiting current plateau. This suggests that diffusion impedance ($W$) increased as the potential increased. So it is very likely that $Cu^{2+}$ is the transport limiting species. Since more $Cu^{2+}$ were produced at

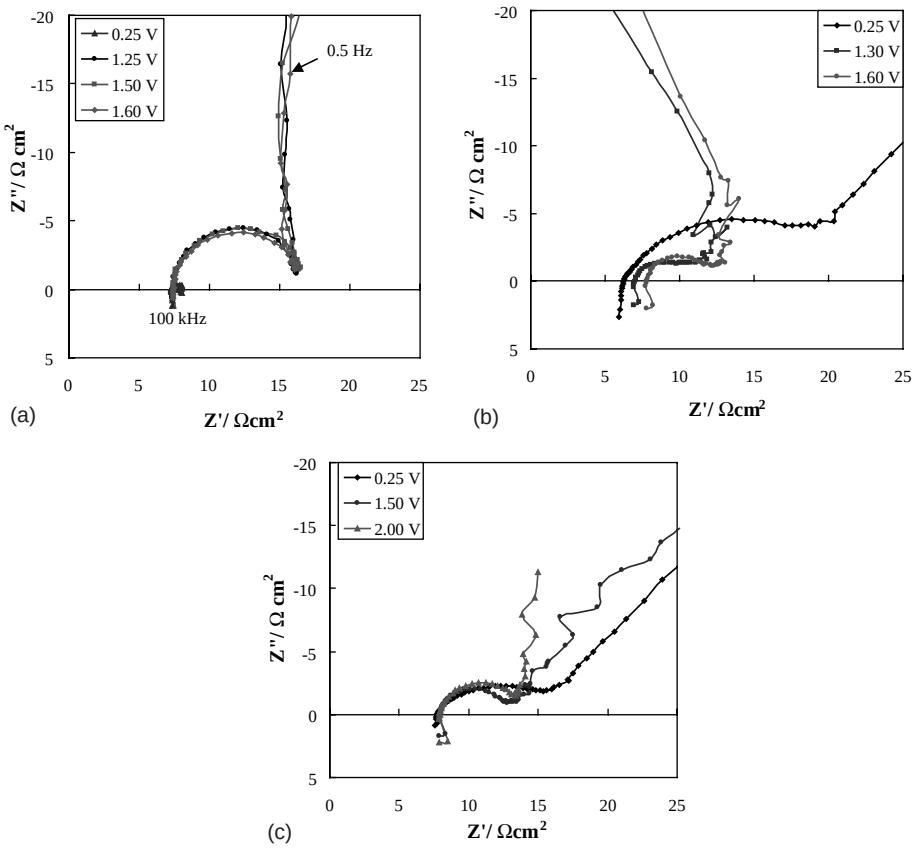


*Fig. 4.* EIS spectra obtained from: (a) 100% phosphoric acid; (b) 70% HEDP; and (c) 70% phosphoric acid + 0.5 M sodium tripolyphosphate solutions.

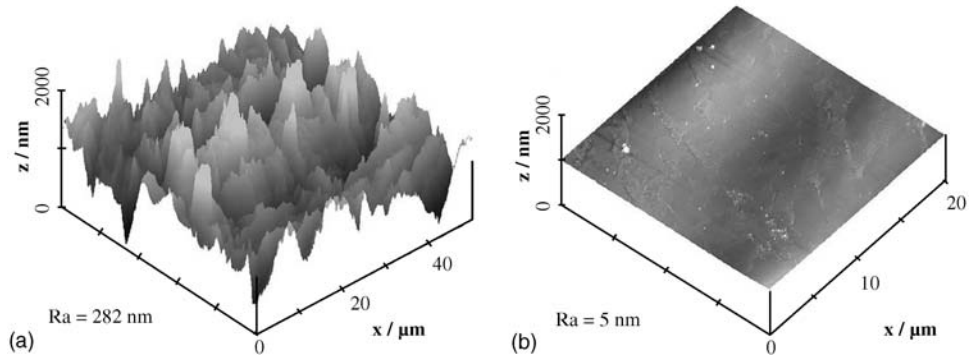


*Fig. 5.* AFM images of copper bulk surface before (a) and after (b) ECP.

higher potential, this resulted in higher concentration gradient in the diffusion layer and thus higher diffusion/migration resistance. However, because the process was mass transport controlled, $Cu^{2+}$ ions produced due to higher potential may not necessarily reach the cathode and complete the charge transfer and current flow cycle. Thus the limiting current did not increase.

By contrast, $R_2$ values of solutions 1 and 2 remain constant at different potentials within the range of the limiting current plateau. This suggests that $Cu^{2+}$ is not the transport limiting species, instead, acceptors, such as anions or water molecules might be the transport limiting species, [10, 11, 20].

The data in Table 1 also shows that the capacitance of all the solutions except solution 4 (HEDP), increased with an increase of potential in the range of the limiting current plateau (0.9 ~ 2.1 V). Capacitance is defined as

$$C = \frac{\mathrm{d}Q}{\mathrm{d}t} \tag{7}$$

where $Q$ is charge and $t$ is time. The driving force of an electrochemical reaction is the electrical potential at the electrode surface. So higher charge transfer (e.g., $Cu - 2e^- \rightarrow Cu^{2+}$ on anode surface) rate is expected at higher potential. Since the process was mass transport

controlled, $Cu^{2+}$ produced due to higher potential may not necessarily reach cathode. Thus, the limiting current (in d.c. mode) did not increase. Instead, more $Cu^{2+}$ entered in the fixed layer and the diffusion layer. Correspondingly, more negative ions were attracted to the diffuse mobile layer. That is, more charges accumulated at the double layer capacitor. Therefore, the capacitance increased under a.c. modulation.

However, in the case of solution 4 (HEDP solution), a salt film formed on the anode surface and its thickness increased with potential in the range of the limiting current plateau. This may also contribute to the capacitance too, since

$$C = \frac{\varepsilon A}{r} \tag{8}$$

where $A$ is the area, $\varepsilon$ and $r$ are the electrical permittivity and thickness of the media between the capacitor plates, respectively. From Equation 8 $C$ decreases with increase in $r$. Therefore, when a thicker salt film was formed at higher potential, the capacitance dropped. This explains why solution 4 has a lower capacitance at 1.6 V than at 1.3 V.

All the solutions in Table 1 have a much higher capacitance at 0.25 V than at potentials in the range of the limiting current plateau. At such a low potential, the double layer is very thin compared to the diffusion layer under mass transport condition. On the other hand, the number of ions in the double layer is also small compared to that under mass transport controlled conditions. Therefore, the capacitance in this case depends on the solution and is very different than that at the limiting current plateau.

### 3.2. *ECP mechanisms of copper discs and EP copper film on deep trench wafers*

The surface roughness of copper discs before and after ECP was measured with an AFM. Typical surface profiles of the copper discs before and after ECP are shown in Figure 5. The best ECP results and Cu removal rate ($R_d$) for each chemical system are listed in Table 2 [14]. The roughness of copper after ECP in HEDP solution could be much larger if the surface film had not been carefully removed. Very good ECP of bulk copper can be achieved with phosphoric acid with (or without) the additives and HEDP solutions under potential control at limiting current.

Nevertheless, the electrochemical polishing of EP copper film on trenched silicon wafers exhibits different characteristics in HEDP and phosphoric acid solutions. Figure 6 shows the surface topography and cross-section of such copper films before and after ECP in phosphoric acid and HEDP solutions. Bumps over dense structures were left behind after ECP of wafer coupons with phosphoric acid. In contrast, a planar surface was produced in HEDP solution. To explain this phenomenon, a better understanding of the ECP mechanisms is required.

#### 3.2.1. *Ohmic levelling*

Levelling can be achieved under ohmic control or mass transport control. Under ohmic control, current density is determined by the electrolyte resistance between the electrodes:

$$J = \frac{V}{\rho_e l} \tag{9}$$

where $V(=V_1-V_0)$ is the potential difference between anode and cathode, $\rho_e$ is the resistivity of the electrolyte, and $l$ is the distance between the cathode and anode. From Equation 10 the current density ($J_P$) at protruding point P is higher than the current density ($J_Q$) at recessed point Q due to the difference ($2b = l_P - l_Q$) of interelectrode distance, as shown in Figure 7.

Surface removal rate (or dissolution rate $R_d$ in cm $s^{-1}$) may be expressed as

$$R_d = \frac{JM}{nFd} \tag{10}$$

where $M$ is the atomic weight (63.5 g for Cu) and $d$ is the density of the anode material (8.96 g $cm^{-3}$ for Cu), $n$ (2 for $Cu - 2e^- \rightarrow Cu^{2+}$ reaction) is the number of electrons transferred in the oxidation reaction of an anode atom, while $F(=96\,485$ C $mol^{-1})$ is the faradaic constant. Substituting Equation 9 into Equation 10, results in

$$R_d = \frac{MV}{nFd\rho_e l} \tag{11}$$

*Table 2.* Mean roughness of copper disc after ECP in various solutions

| Solution | Limiting current, $i_L$/mA | Time, t/s | Cu removal rate, $R_d/\mu$m $min^{-1}$ | Roughness, $R_a$/nm |
|---|---|---|---|---|
| 1. 70∼100% phosphoric acid | 12∼50 | 2000 | 0.26∼1.10 | 4∼9 |
| 2. 70% phosphoric acid + 0.5 M CuO | 45 | 500 | 0.99 | 5 |
| 3. 70% phosphoric acid + 5% ethylene glycol | 46 | 500 | 1.01 | 5 |
| 4. 70% HEDP | 30 | 800 | 0.66 | 6 |
| 5. 70% phosphoric acid + 0.1 M sodium tripolyphosphate | 40 | 600 | 0.88 | 7 |
| 6. 30% ethylene glycol + 2 M sodium chloride | 50 | 500 | 1.10 | 63 |
| 7. 20% sulfuric acid + 0.1 potassium nitrate | 70 | 300 | 1.54 | 72 |

Note: phosphoric acid = 85% $H_3PO_4$.

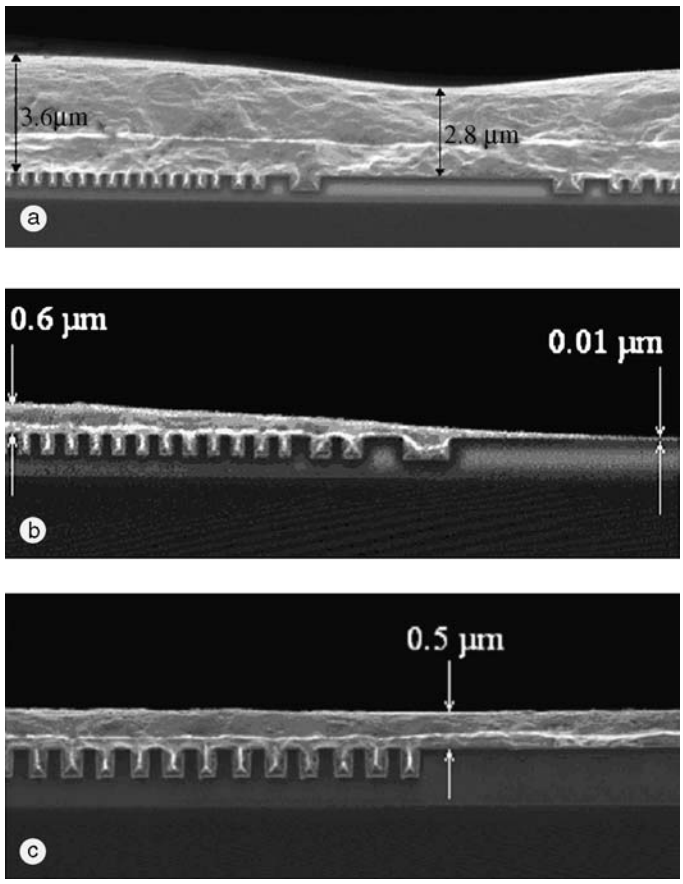


*Fig. 6.* AFM tomography images of electroplated copper films on trenched silicon substrate before ECP (a) and after ECP in phosphoric acid (b) and in HEDP (c) solutions.

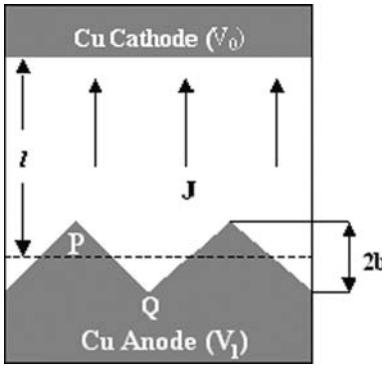


*Fig. 7.* On a rough anode surface with uniform potential ($V_1$), peaks have higher current density due to different interelectrode distance: $l_P > l_Q$.

For given electrode potential, anode material, and reaction, $MV/(nFd) = f$ is a constant. Therefore, ohmic levelling, the difference in the removal rate between protruding point (P) and recessed point (Q), depends on the surface profile and can be expressed as

$$\Delta R_d = R_d(P) - R_d(Q) = f\frac{2b}{\rho_e(l^2 - b^2)} \qquad (12)$$

Equation 12 indicates that larger surface roughness, closer electrode spacing (i.e., smaller $l$), and smaller electrolyte resistivity should produce better levelling effects.

Assuming $\rho_e = 10\ \Omega$ cm [23], $2b = 0.5\ \mu$m, $l = 20$ cm, and $V = 2$ V, gives $\Delta R_d = 9.18 \times 10^{-9}\ \mu$m s$^{-1}$, which is negligible compared to the average removal rate $R_d = 4.4 \times 10^{-3}\ \mu$m s$^{-1}$ at a limiting current $i_L$ of 12 mA for 85% $H_3PO_4$ solution. This indicates that the ohmic levelling effect is negligible under normal wafer ECP conditions, if an anode layer does not exist or if the layer conforms to the surface (i.e., microprofile).

Nevertheless, ohmic levelling effect can be remarkable under certain hydrodynamic conditions, if a nonconformal anodic layer with a flat layer–electrolyte interface (i.e., macroprofile) is formed on the anode surface (Figure 8). In this case, the current density is determined

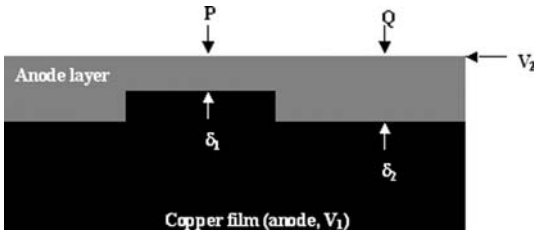


*Fig. 8.* Salt film with macroprofile formed on anode surface facilitates surface smoothing due to ion migration/diffusion and/or ohmic levelling effect.

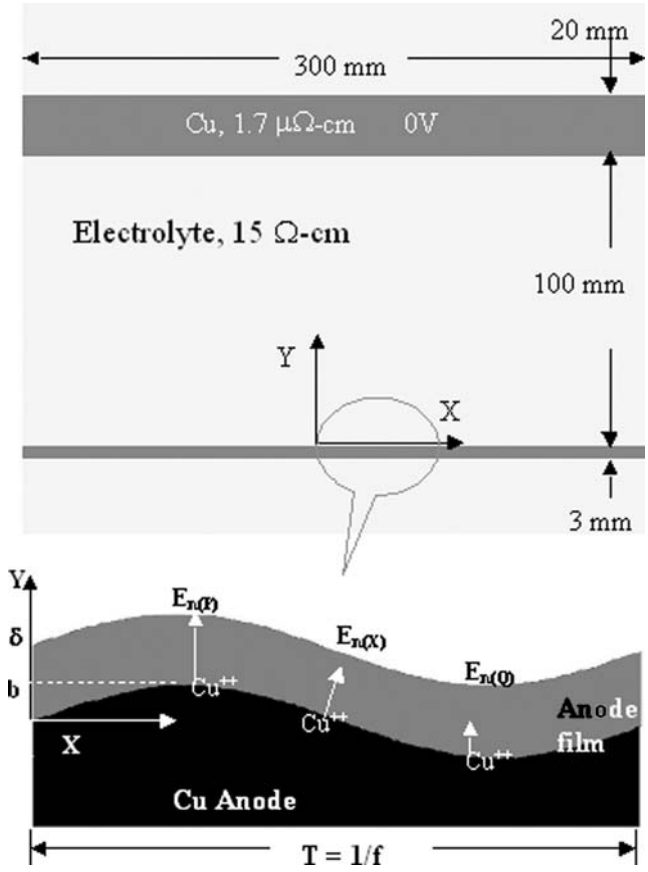


*Fig. 9.* Schematic of an electropolishing cell and the local surface profile of the anode. Electric field ($E$) varies in amplitude and orientation along the sinusoidal surface.

by the anode layer, since the process is mass transport controlled by the anode layer. Thus, from Equations 12 and 12 we obtain

$$\Delta R_{\mathrm{d}} = R_{\mathrm{d}}(\mathrm{P}) - R_{\mathrm{d}}(\mathrm{Q}) = f\frac{\delta_2 - \delta_1}{\rho_f \delta_1 \delta_2} \tag{13}$$

where $\rho_{\mathrm{f}}$ is the electrical resistivity of the anode layer, $\delta_1$ and $\delta_2$ are the thickness of the anode layer at points P and Q, respectively (Figure 8). Assuming $\delta_2 = 0.5$ $\mu$m, $\delta_1 = 0.25$ $\mu$m, $\rho_{\mathrm{f}} = 2 \times 10^4$ $\Omega$ cm (estimated from the above EIS measurement, in the case of 70% HEDP solution), and $V = V_2 - V_1 = 0.2$ V (voltage across the anode layer), we calculated $\Delta R_{\mathrm{d}} \approx 0.07$ $\mu$m s$^{-1}$, according to Equation 14. In comparison, the average removal rate $R_{\mathrm{d}}$ is 0.01 $\mu$m s$^{-1}$ at limiting current $i_{\mathrm{L}} = 30$ mA for 70% HEDP solution. In other words, the removal rate at protruding point (P) is about seven times higher than the average removal rate on the flat area due to ohmic levelling effect. The ohmic levelling effect can be enhanced by increasing the overall thickness of the anode layer and lowering its resistivity according to Equation 13. Under mass transport conditions, increasing anodic potential also increases the ohmic levelling effect according to the above equations. >

3.2.2. *Migration smoothing*

Another geometrical-dependent levelling mechanism results from migration. It is known that an arbitrary two-dimensional surface profile can be described by a Fourier sine series where the individual Fourier coefficients behave independently [3]. Therefore the electric field distribution along a sinusoidal surface was calculated where a sine waveform is located at the center of the anode surface in a 2D electrochemical cell, which has parameters close to an actual 300 mm wafer polishing system (Figure 9). This simulation was performed using boundary element simulation software. The simulation results (Figure 10) indicate that the amplitude of normal

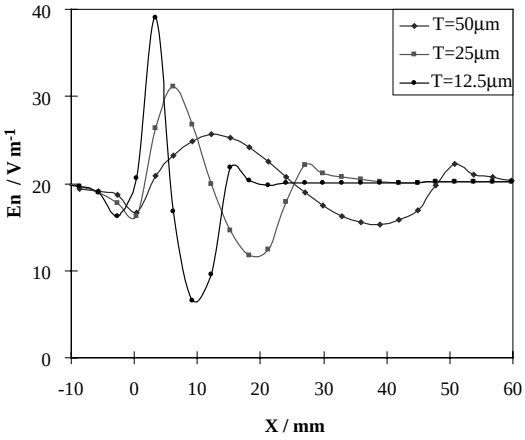


*Fig. 10.* Amplitude of normal electric field along the sinusoidal anode surface, obtained by simulation.

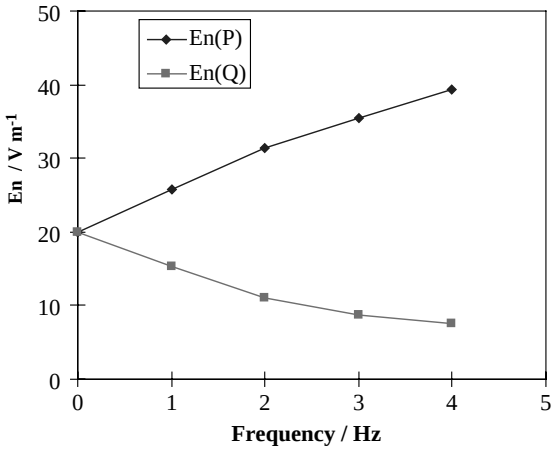


*Fig. 11.* Amplitude of normal electric field $E_n$(P) at the peak and $E_n$(Q) at the valley of the sinusoidal surface, against the frequency of the sine wave.

electric field ($\mathbf{E_n}$) varies along the sinusoidal surface, similar to the shape of the surface profile except at the origin and end points of the sine waveform where a sharp geometric change occurs. For a certain amplitude ($b$) of the sine wave, the difference in the normal electric field $\mathbf{E_n}$(P) at the peak point P and $\mathbf{E_n}$(Q) at the recessed point Q increases as the wavelength ($T$) decreases (i.e., the frequency $f$ increases), as indicated in Figure 11. The orientation of the normal electric field also depends on the location. At peaks and valleys, (points P and Q), $\mathbf{E_n}$ points perpendicular to the cathode, and deviates from this direction at other locations.

Once a copper atom is oxidized to $Cu^{2+}$ on the anode surface, a force ($\mathbf{F_E}$) acts on the $Cu^{2+}$ resulting from the electric field $\mathbf{E_n}$. As a result, $Cu^{2+}$ tend to move away from the anode surface towards the cathode under the force:

$$\mathbf{F} = \mathbf{F_E} - \mathbf{F_r} = \mathbf{qE} - \mathbf{F_r} \tag{14}$$

where $q$ is the charge of $Cu^{2+}$ and $\mathbf{F_r}$ is the resistive force as $Cu^{2+}$ move through the anode film and the solution. Accordingly, the $Cu^{2+}$ accelerate at $\mathbf{a} = \mathbf{F}/m$ and move with a velocity

$$v = \frac{1}{2}\frac{F}{m}t = \frac{1}{2m}(qE_n - F_r)t \tag{15}$$

where $m$ is the mass of $Cu^{2+}$and $t$ is time.

In bulk solution $F_E$ is negligible compared to the convection force ($F_c$) when a forced convection is applied by stirring or circulation. In an electrically resistive anode layer, $Cu^{2+}$ migration is the limiting process of mass transport. Thus, the surface removal rate $R_d$ is proportional to $v$, that is, $R_d = \alpha v$ (where $\alpha$ is a constant). The difference in the removal rate between protruding point (P) and recessed point (Q) is

$$\Delta R_d = \alpha(v_P - v_Q) = \frac{\alpha q}{2m}[E_n(P) - E_n(Q)]t \tag{16}$$

From Equation 16 and Figure 11 it may concluded that ECP, due to ion migration, leads to a surface profile of longer waves that disappear slower than the shorter waves.

#### 3.2.3. *Diffusion smoothing*

The ECP effect due to diffusion, driven by the concentration gradient, has the same tendency. The details were discussed by Wagner [20], who calculated the dissolution rate of copper using Fick's second law, under mass transport control and acceptor mechanism conditions.

#### 3.2.4. *Interpretation of ECP results*

According to the above discussion, better ECP can be achieved at sharper geometrical profiles, due to ion migration or diffusion. This explains why a very good ECP effect was obtained from all the solutions with copper discs, having sharp surface profiles (Figure 5(a)). The ECP effect is considerably reduced in the case of EP copper film on a patterned wafer, due to the gentle surface undulation, and/or due to lack of ion migration (e.g., water molecules instead of Cu ions as the mass transport control species).

However, the situation changes when an electrically resistive film with macroprofile is formed on the anode surface. In this case, as shown in Figure 8, $Cu^{2+}$ migration at protruding areas has a shorter distance to reach bulk solution than that at recessed areas. Therefore, an ECP effect can be achieved even when the surface profile has only gentle undulations.

The surface profile of the anode layer depends on the viscosity of the layer and the convection strength of the electrolyte. A macroprofile is a favourable condition for ECP of any surface, whereas a microprofile only favours the ECP of a shorter wave surface.

Mass transport control is the prerequisite condition. For this reason, potential control is the technique normally used to guarantee mass transport conditions due to a wide operation window ($E_L$). Comparatively, current control [24] is seldom used, as it is difficult to maintain the mass transport condition since there is no operating window ($i_L$).

## 4. Conclusions

Copper anodic layers in solutions of HEDP, phosphoric acid, and phosphoric acid with organic and inorganic additives were analysed *in situ* using EIS. Analysis of the impedance spectra suggested that a salt film was formed on the copper anode surface in HEDP while no salt film was formed in the other solutions. Analysis from the impedance data also suggested that $Cu^{2+}$ was the mass transport controlling species in solutions of HEDP and phosphoric acid with additives ethylene glycol and sodium tripolyphosphate. Water molecules are probably the mass transport controlling species in solutions of phosphoric acid and phosphoric acid with copper oxide.

Very good electropolishing results (surface mean roughness $R_a < 10$ nm) of bulk copper were obtained in all the solutions studied. But electropolishing of EP copper films on patterned silicon wafers showed different results. Gently protruding areas were not planarized in an ECP process with phosphoric acid while good planarization was obtained in HEDP solutions.

The ECP effect is sensitive to the surface profiles of the anode substrate and anodic layers. The microprofile of anodic layer favours the ECP of surface profiles that involve shorter wavelength, whereas a macroprofile of an anodic layer can planarize any surface profile.

## Acknowledgements

The authors acknowledge Ms Nancy Zelick at Intel Corporation and Mr Jay Jordan at FEI Company for their assistance in preparing wafer samples and their SEM images.

## References

1. R. Soutebin and D. Landolt, *J. Electrochem. Soc.* **129** (1982) 946.
2. R. Soutebin H. Froidevaux and D. Landolt, *J. Electrochem. Soc.* **127** (1982) 1096.
3. D. Landolt, *Electrochim. Acta* **32** (1987) 1.
4. H. Abrams and C.L. Mantell, *Electrochem. Tech.* **5** (1967) 287.
5. M. Matlosz, S. Magaino and D. Landolt, *J. Electrochem. Soc.* **141** (1994) 410.
6. S. Sato, Z. Yasuda, M. Ishihara, N. Komai, H. Ohtorii, A. Yoshio, Y. Segawa, H. Horikoshi, Y. Ohoka, K. Tai, S. Takahashi and T. Nogami, 0-7803-7052-X/01 (IEEE 2001).
7. M.H. Tsai, S.W. Chou, C.L. Chang, C.H. Hsieh, M.W. Lin, C.M. Wu, W.S. Shue, D.C. Yu and M.S. Liang, 'Technical Digest of the International Electron Devices Meeting', Washington DC (Dec. 2001), p. 4.3.1 (IEEE 2001).
8. M. Datta, *IBM J. Res. Develop.* **42** (1998) 655.
9. S-C. Chang, J-M. Shieh, C-C. Huang, B-T. Dai and M-S. Feng, *Jpn. J. Appl. Phys.* **41** (2002) 7332.
10. S-C. Chang, J-M. Shieh, C-C. Huang, B-T. Dai, Y-H. Li and M-S. Feng, *J. Vac. Sci. Technol. B* **20** (2002) 2149.
11. R. Vidal and A.C. West, *J. Electrochem. Soc.* **142** (1995) 2682.
12. S. Magaino, M. Matlosz and D. Landolt, *J. Electrochem. Soc.* **140** (1993) 1365.
13. R.D. Grimm, A.C. West and D. Landolt, *J. Electrochem. Soc.* **139** (1992) 1622.
14. J. Huo, 'Electrochemical Planarization of Copper for Microelectronic Applications', doctoral dissertation (OGI of Science and Engineering, Oregon Health and Science University, Beaverton, Oregon, 2003).
15. A.J. Bard and L.R. Faulkner, 'Electrochemical Methods Fundamentals and Application', (J. Wiley & Sons, New York, 2nd edn, 2001), p. 137.
16. F.P. Incropera and D.P. DeWitt, 'Fundamentals of Heat and Mass Transfer', (J. Wiley & Sons, New York, 4th edn, 1996), pp. 294–351.
17. A.J. Bard and L.R. Faulkner: 'Electrochemical Methods Fundamentals and Application', (J. Wiley & Sons, New York, 2nd edn, 2001), p. 141.
18. A.J. Bard and L.R. Faulkner: 'Electrochemical Methods Fundamentals and Application', (J. Wiley & Sons, New York, 2nd edn, 2001), p. 611.
19. J. Koryta, J. Dvorak and L. Kavan, 'Principles of Electrochemistry', (J. Wiley & Sons, New York, 2nd edn, 1993), pp. 301–303.
20. C. Wagner, *J. Electrochem. Soc.* **101** (1954) 225.
21. J.L. Fang and N.J. Wu, *J. Electrochem. Soc.* **136 (**1989) 3800.
22. J. Huo, R. Solanki and J. McAndrew, *Surf. Eng.* **19 (**2003) 11.
23. K. Dianatkhah, 'Passivation Behavior of Copper Thin Films for Electrochemical Planarization Application', MS thesis, (Oregon Graduate Institute of Science and Technology, Beaverton, Oregon, 1999).
24. D. Padhi, J. Yahalom, S. Gandikota and G. Dixit, *J. Electrochem. Soc.* **150** (2003) G10.